

UCSF

UC San Francisco Previously Published Works

Title

The C. elegans homolog of human panic-disorder risk gene TMEM132D orchestrates neuronal morphogenesis through the WAVE-regulatory complex

Permalink

<https://escholarship.org/uc/item/2ds8c4f7>

Journal

Molecular Brain, 14(1)

ISSN

1756-6606

Authors

Wang, Xin

Jiang, Wei

Luo, Shuo

et al.

Publication Date

2021-12-01

DOI

10.1186/s13041-021-00767-w

Copyright Information

This work is made available under the terms of a Creative Commons Attribution License, available at <https://creativecommons.org/licenses/by/4.0/>

Peer reviewed

RESEARCH

Open Access



The *C. elegans* homolog of human panic-disorder risk gene *TMEM132D* orchestrates neuronal morphogenesis through the WAVE-regulatory complex

Xin Wang^{1,2†}, Wei Jiang^{3†}, Shuo Luo¹, Xiaoyu Yang⁴, Changnan Wang¹, Bingying Wang¹, Yongjun Dang³, Yin Shen⁴ and Dengke K. Ma^{1*} 

Abstract

TMEM132D is a human gene identified with multiple risk alleles for panic disorders, anxiety and major depressive disorders. Defining a conserved family of transmembrane proteins, *TMEM132D* and its homologs are still of unknown molecular functions. By generating loss-of-function mutants of the sole *TMEM132* ortholog in *C. elegans*, we identify abnormal morphologic phenotypes in the dopaminergic PDE neurons. Using a yeast two-hybrid screen, we find that NAP1 directly interacts with the cytoplasmic domain of human *TMEM132D*, and mutations in *C. elegans tmem-132* that disrupt interaction with NAP1 cause similar morphologic defects in the PDE neurons. NAP1 is a component of the WAVE regulatory complex (WRC) that controls F-actin cytoskeletal dynamics. Decreasing activity of WRC rescues the PDE defects in *tmem-132* mutants, whereas gain-of-function of *TMEM132D* in mammalian cells inhibits WRC, leading to decreased abundance of select WRC components, impaired actin nucleation and cell motility. We propose that metazoan *TMEM132* family proteins play evolutionarily conserved roles in regulating NAP1 protein homologs to restrict inappropriate WRC activity, cytoskeletal and morphologic changes in the cell.

Keywords: *TMEM132D*, Panic disorder, WAVE regulatory complex, Actin, *C. elegans*

Introduction

Despite decades of genetic and molecular analyses, the genome of the common model organism *C. elegans* still comprises many functionally uncharacterized genes [1–4]. One such example is the *C. elegans* gene *Y71H2AM.10*, an ortholog of the evolutionarily conserved *TMEM132* gene family [1, 5]. This family encodes single-pass transmembrane proteins present in metazoans but remains functionally uncharacterized in

any organisms. The human genome encodes 5 paralogs (*TMEM132A-E*), genetic variants of which have been identified as risk alleles of many human diseases, including those associated with panic disorder and anxiety severity in *TMEM132D* [6–12]. Risk variants of *TMEM132D* have been shown to correlate with altered mRNA levels of *TMEM132D* in anxiety-related brain regions and psychiatric syndromes [6, 9]. In addition, the *TMEM132D* locus in cattle appears to have undergone an evolutionary selective sweep during domestication, along with reduced fearfulness in cattle's behaviors [13]. The expression of *TMEM132* family genes is also highly enriched in the nervous system of diverse animals, including *C. elegans* and humans [14, 15]. However, it remains unknown how *TMEM132* family proteins

*Correspondence: Dengke.Ma@ucsf.edu

[†]Xin Wang and Wei Jiang contributed equally to this work

¹ Cardiovascular Research Institute and Department of Physiology, University of California San Francisco, San Francisco, CA 94158, USA
Full list of author information is available at the end of the article



regulate neuronal structure and function and how their abnormal function and regulation may contribute to various neurological and psychiatric diseases.

Neuronal morphological changes are driven primarily by actin cytoskeletal dynamics under the control of the WAVE-regulatory complex (WRC). WRC promotes actin nucleation to form filamentous actin (F-actin) by stimulating activity of the Arp2/3 complex in response to biochemical signals originating from a variety of neuronal membrane receptors [16–18]. WRC is a multi-subunit complex comprising SRA1, HSPC300, ABI1/2, WAVE1/2 and NAP1 (also known as NCKAP1) proteins. *NAP1* was initially identified as a gene with strongly decreased expression in the brain of patients with sporadic Alzheimer's disease [19]. Deleterious *NAP1* variants were also identified in human patients with autism and intellectual disability [20, 21]. Among other components in the WRC, the SRA and ABI proteins form an evolutionarily conserved binding interface for diverse WRC ligands that commonly contain the WRC-interacting receptor sequence (WIRS) motif [16, 17]. Whether *NAP1* directly interacts with any neuronal membrane receptors to affect WRC signaling and actin cytoskeletal changes has not been reported. It has also been unclear how WRC abundance is regulated in cell compartments where actin nucleation needs to be limited in morphologically complex cells, including neurons.

To elucidate biological functions and mechanisms of action of TMEM132 family proteins, we generated and characterized *C. elegans* loss-of-function (LOF) mutations in *Y71H2AM.10*, the sole ortholog of the *TMEM132* gene family. We found that *tmem-132* mutants exhibit striking morphological defects in the dopaminergic PDE neurons. Human *NAP1* binds to *TMEM132D* and their *C. elegans* homologs also interact with each other. Genetic interactions between *tmem-132* and WRC-encoding genes in regulating PDE morphology, the LOF phenotype of *tmem-132* mutants and gain-of-function (GOF) phenotype of *TMEM132D* in mammalian cells collectively suggest that *TMEM132* family proteins may regulate *NAP1* in WRC to finely modulate actin nucleation, cellular cytoskeletal and morphological changes.

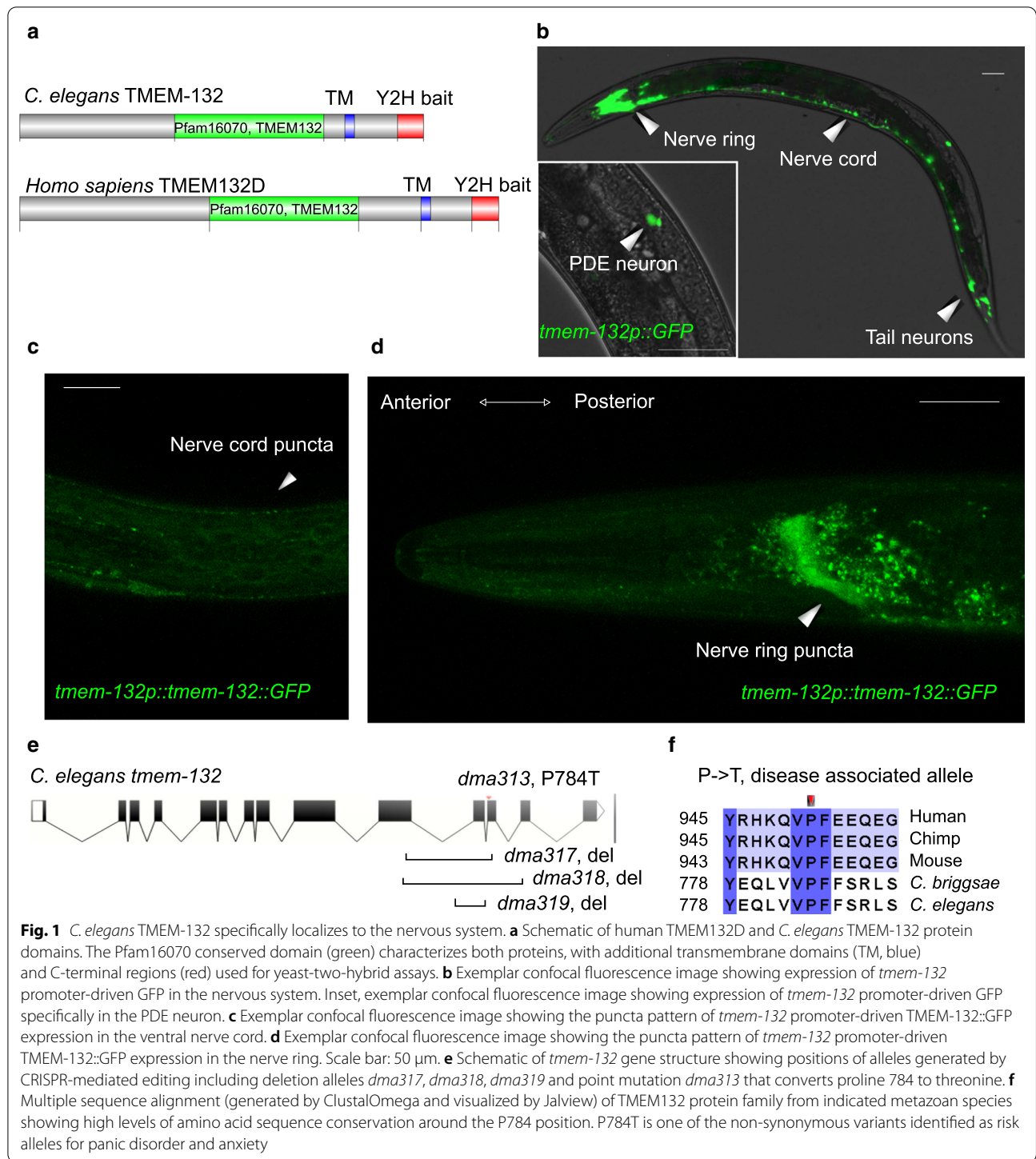
Results

The *C. elegans* *TMEM-132* localizes to neurons and regulates the dopaminergic PDE neuron morphology

Protein homology and motif analysis identified the Pfam16070 domain characteristic of both human *TMEM132D* and *C. elegans* *TMEM-132*, classifying them to the evolutionarily conserved *TMEM132* protein superfamily (Fig. 1a and Additional file 1: Fig. S1). A translational reporter that fuses *tmem-132* with

GFP revealed enriched expression of *C. elegans* *tmem-132* in neurons (Fig. 1b–d), implicating a specific role of *TMEM-132* in the nervous system. Lack of mammalian loss-of-function models and potential genetic redundancy among the *TMEM132A-E* family members precluded us from analyzing the physiological function of *TMEM132D* in vivo. Thus, we sought to address this issue in *C. elegans*, which encodes *tmem-132* as the sole ortholog of the gene family and has served as excellent model to study neuronal cell biology [22–24]. We used CRISPR-Cas9 techniques to generate a series of *C. elegans* mutants, including multiple independently-derived deletions, an early stop-codon mutant and a genetic P784T knock-in mutant, in which the highly conserved proline residue became threonine, corresponding to the human disease risk allele for anxiety and panic disorders (Fig. 1e, f). We generated such multiple independent mutations to seek convergent phenotype and outcrossed all mutants to eliminate potential interference of phenotype by background mutations.

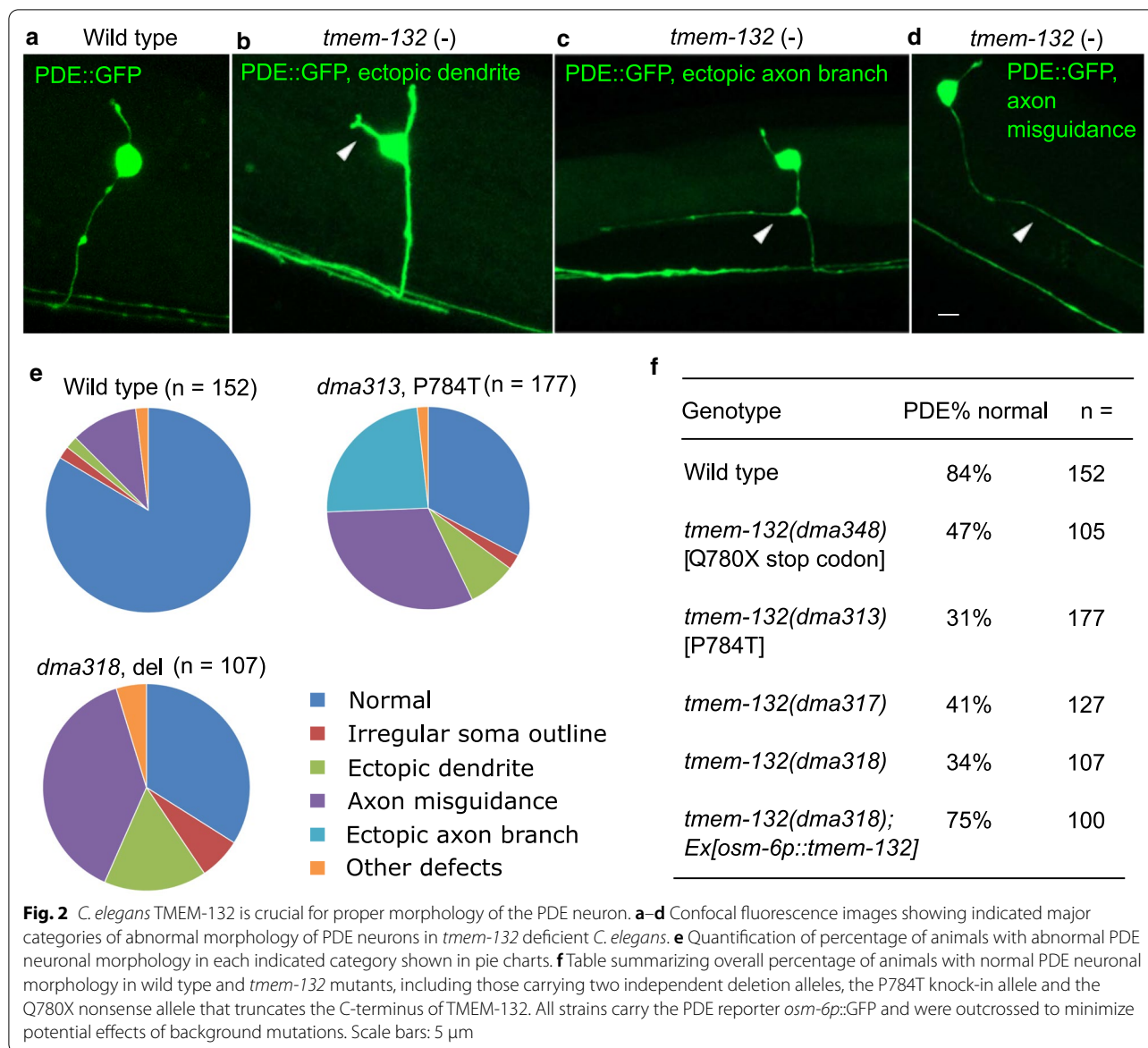
Given the exclusive localization of *TMEM-132* in neurons, we subjected *tmem-132* mutants to a variety of neuronal phenotypic analyses. We did not observe gross behavioral defects under normal conditions. We next crossed the mutants to various established GFP reporters to examine neurons of stereotyped morphology, including ciliated sensory AWC neurons, hermaphrodite-specific HSN neurons, mechanosensory PVD, ADE and PDE neurons (Additional file 1: Fig. S2). Among the neurons examined, the dopaminergic neuron PDE exhibited the most severe defect, thus in this study we focused on PDE, which is marked by the *osm-6p::GFP* reporter in addition to other ciliated and dopaminergic neurons. Although dense GFP signals prevented us from analyzing the anterior group of ciliated and dopaminergic neurons, close confocal microscopic analysis of the posterior, anatomically isolated PDE neurons revealed striking abnormal morphologies in a large fraction of *tmem-132* mutants (Fig. 2a–d). We categorized the mutant phenotype into several classes, including those with irregular soma outlines, ectopic dendrites, ectopic axon branches, and axon misguidance as similarly described previously [25, 26]. Although the phenotypic defects of PDE are diverse, all mutants show similar profiles in distribution of different categories of phenotypic defects (Fig. 2e, f). *tmem-132* LOF mutants also exhibited morphological defects in the ADE and PVD but not morphologically less complex AWC neurons (Additional file 1: Fig. S2). Neuronal morphogenesis critically depends on neuronal interactions with glia and epithelia in *C. elegans* [23, 27, 28]. Importantly, transgenic expression of *tmem-132* driven by the *osm-6* promoter rescued the morphologic defect



of *tmem-132* mutants, indicating a causal and cell-autonomous role of TMEM-132 for ensuring normal PDE neuronal morphology (Fig. 2f).

Human TMEM132D interacts with the WRC component NAP1

To begin to understand molecular functions of this conserved protein superfamily, we used yeast-two-hybrid (Y2H) screens to identify protein interactors of human TMEM132D. The predicted intracellular C-terminus of



TMEM132D contains cytoplasmic motifs likely related to actin cytoskeletal dynamics [5, 16]. We thus constructed a yeast bait vector expressing its C-terminal domain and used the bait to screen for interactors from a human-cDNA prey library. We also constructed a bait vector that contains the homologous C-terminus of *C. elegans tmem-132* and focused on identified screen hits whose homologs can interact with human and *C. elegans* baits, respectively. From 117 independent cDNA clones isolated and identified by Sanger sequencing (Additional file 2: Table S1), we found that the protein NAP1 encoded by *NCKAP1* showed robust interaction with TMEM132D in Y2H assays (Fig. 3a). NAP1 is an integral component of the WAVE regulatory complex that regulates actin

nucleation and cytoskeletal changes in the cell through the ARP2/3 complex [16, 18, 29, 30]. We found that GEX-3, the *C. elegans* ortholog of NAP1, also interacts with the C-terminus of *C. elegans* TMEM-132 (Fig. 3a).

In addition to NAP1, the WRC also contains three other major proteins SRA1, ABI1/2 and WAVE1/2, with corresponding orthologs *gex-2*, *abi-1* and *wve-1* in *C. elegans* (Fig. 3b) [17, 25, 31]. We verified the biochemical interaction between full-length NAP1 and TMEM132D in mammalian cells by co-immunoprecipitation (CoIP) assays. GFP-tagged NAP1, when expressed in heterologous HEK293 cells with V5 epitope-tagged TMEM132D, was able to pull down TMEM132D in CoIP (Fig. 3c). Another component of WRC, SRA1, is

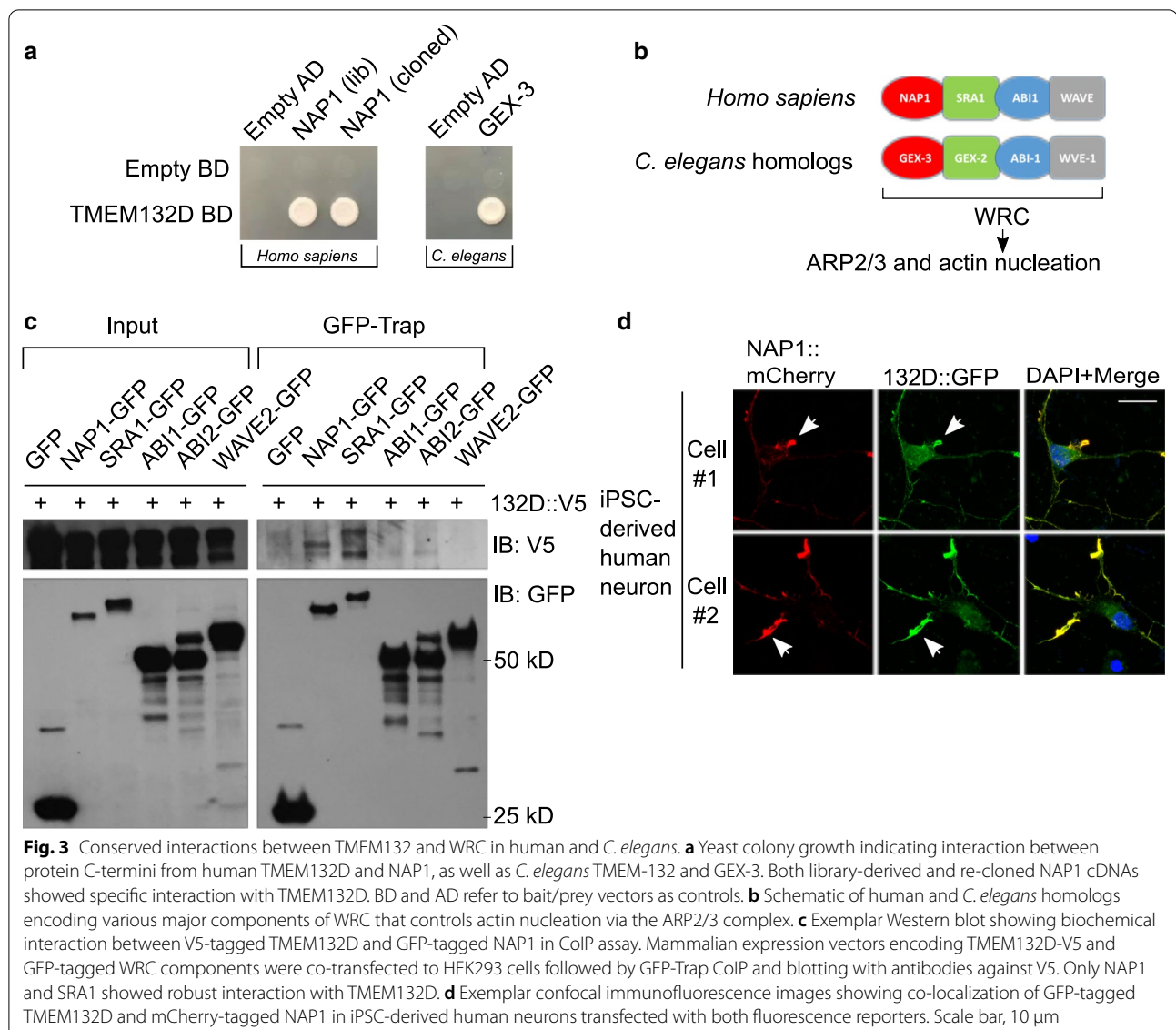
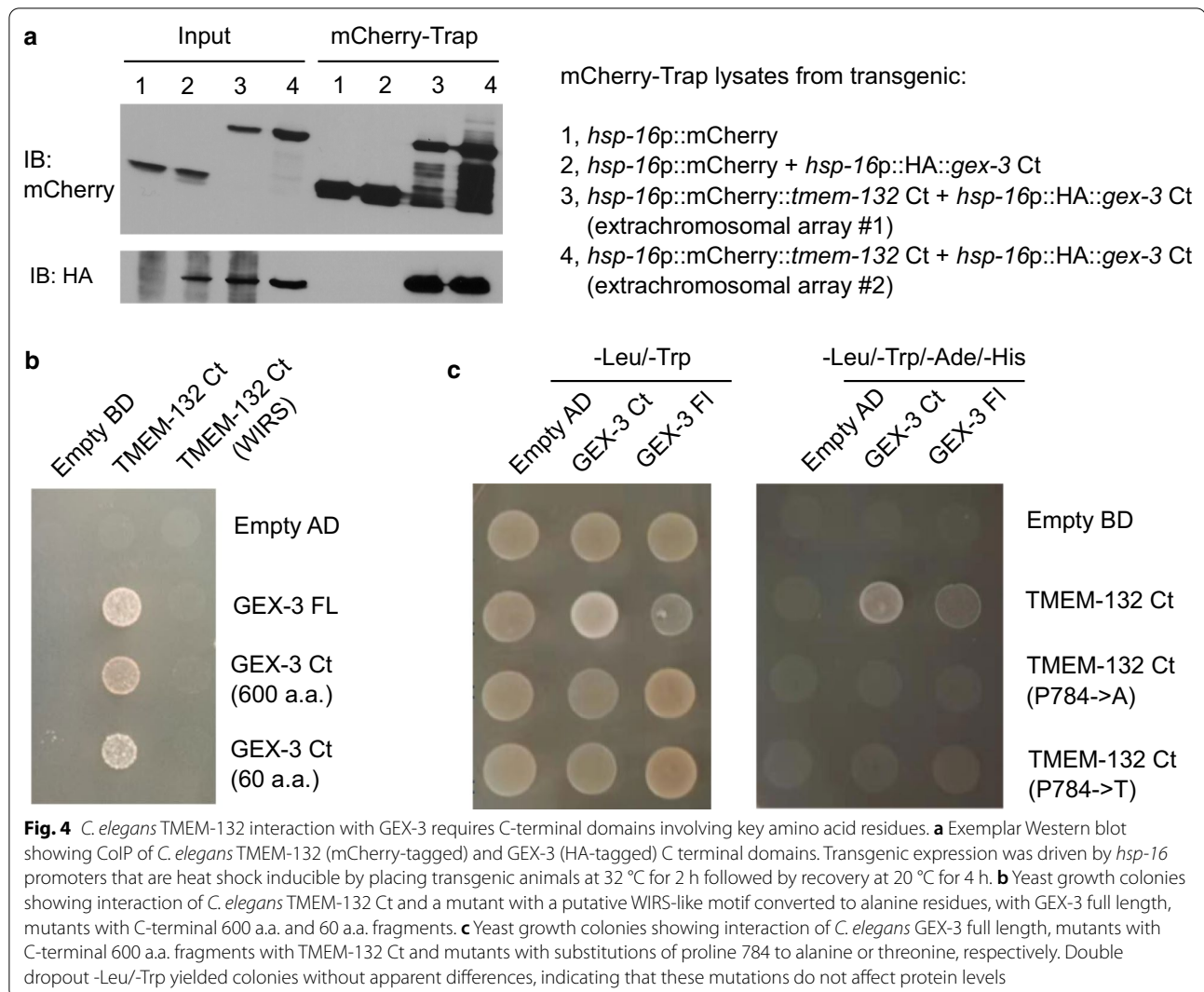


Fig. 3 Conserved interactions between TMEM132 and WRC in human and *C. elegans*. **a** Yeast colony growth indicating interaction between protein C-termini from human TMEM132D and NAP1, as well as *C. elegans* TMEM-132 and GEX-3. Both library-derived and re-cloned NAP1 cDNAs showed specific interaction with TMEM132D. BD and AD refer to bait/prey vectors as controls. **b** Schematic of human and *C. elegans* homologs encoding various major components of WRC that controls actin nucleation via the ARP2/3 complex. **c** Exemplar Western blot showing biochemical interaction between V5-tagged TMEM132D and GFP-tagged NAP1 in CoIP assay. Mammalian expression vectors encoding TMEM132D-V5 and GFP-tagged WRC components were co-transfected to HEK293 cells followed by GFP-Trap CoIP and blotting with antibodies against V5. Only NAP1 and SRA1 showed robust interaction with TMEM132D. **d** Exemplar confocal immunofluorescence images showing co-localization of GFP-tagged TMEM132D and mCherry-tagged NAP1 in iPSC-derived human neurons transfected with both fluorescence reporters. Scale bar, 10 μ m

structurally similar to NAP1 and together with NAP1 forms a heterodimeric sub-complex in WRC [30]. GFP-tagged SRA1 also pulled down TMEM132D, although we did not observe apparent association of TMEM132D with other components of WRC. When co-expressed in fully differentiated human neurons derived from induced pluripotent stem cells (iPSC), GFP-tagged TMEM132D markedly co-localized with mCherry-tagged NAP1 (Fig. 3d). Collectively, these genetic, biochemical and cellular imaging results identify NAP1 as a protein interactor of TMEM132D and indicate that such interaction is evolutionarily conserved also for *C. elegans* counterparts.

The C-terminal domain and the conserved P784 are required for the interactions between TMEM132 and WRC components

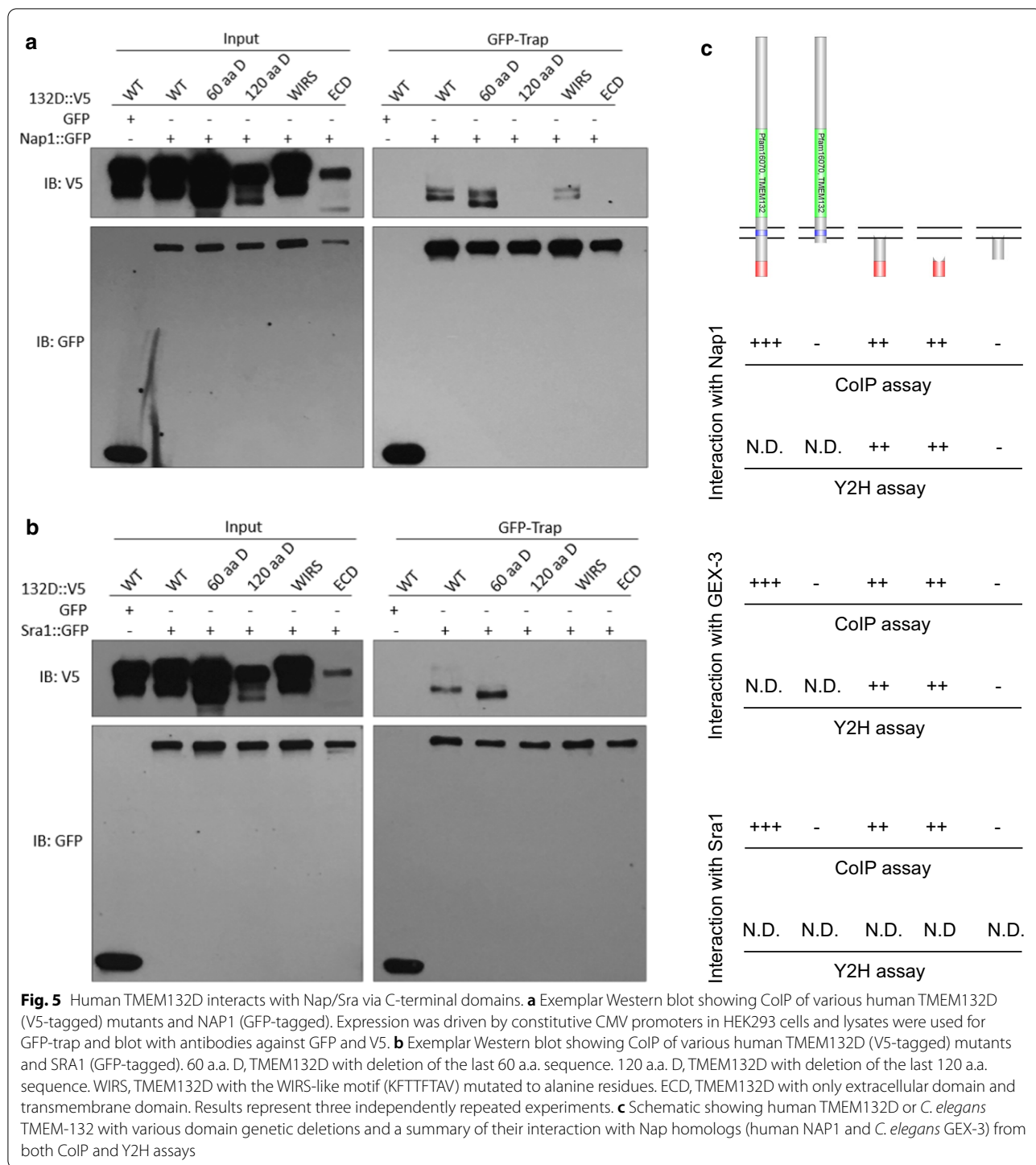
We used Y2H and CoIP assays to further define the C-terminal domain of human TMEM132D or *C. elegans* TMEM-132 that is crucial for interacting with C-termini of NAP1 homologs. To examine interaction between GEX-3 (*C. elegans* NAP1 homolog) and TMEM-132, we generated transgenic strains in which HA epitope-tagged GEX-3 and mCherry-tagged TMEM-132 Ct are co-induced by heat shock promoters (Fig. 4a). Using the mCherry-Trap CoIP assay, we found that mCherry-tagged TMEM-132 Ct specifically pulled down HA epitope-tagged GEX-3, compared with heat shock-induced mCherry only as control (Fig. 4a). We also



confirmed interaction between GEX-3 Ct and TMEM-132 Ct in Y2H assays, in which the most C-terminal 60 a.a. of GEX-3 was sufficient to mediate the interaction (Fig. 4b). In the C-terminus homologous to the WIRS-containing TMEM132D, mutation of a WIRS-like motif attenuated TMEM-132 interaction with GEX-3 (Fig. 4b). Furthermore, we generated mutations to convert the conserved proline 784 to alanine or threonine (to model psychiatric disorder-associated risk allele in humans, see Fig. 1f) in TMEM-132 and found that both mutations abolished the interaction with GEX-3 (Fig. 4c).

Previous studies revealed that the WIRS of diverse transmembrane proteins in mammals mediates binding to an interaction surface of WRC [16]. As TMEM132D contains such a motif at its C-terminus, we performed mutation analysis in Co-IP assays and found that deletion of the entire cytoplasmic portion, deletion of the 120 a.a. C-terminus or mutation of the WIRS-like motif

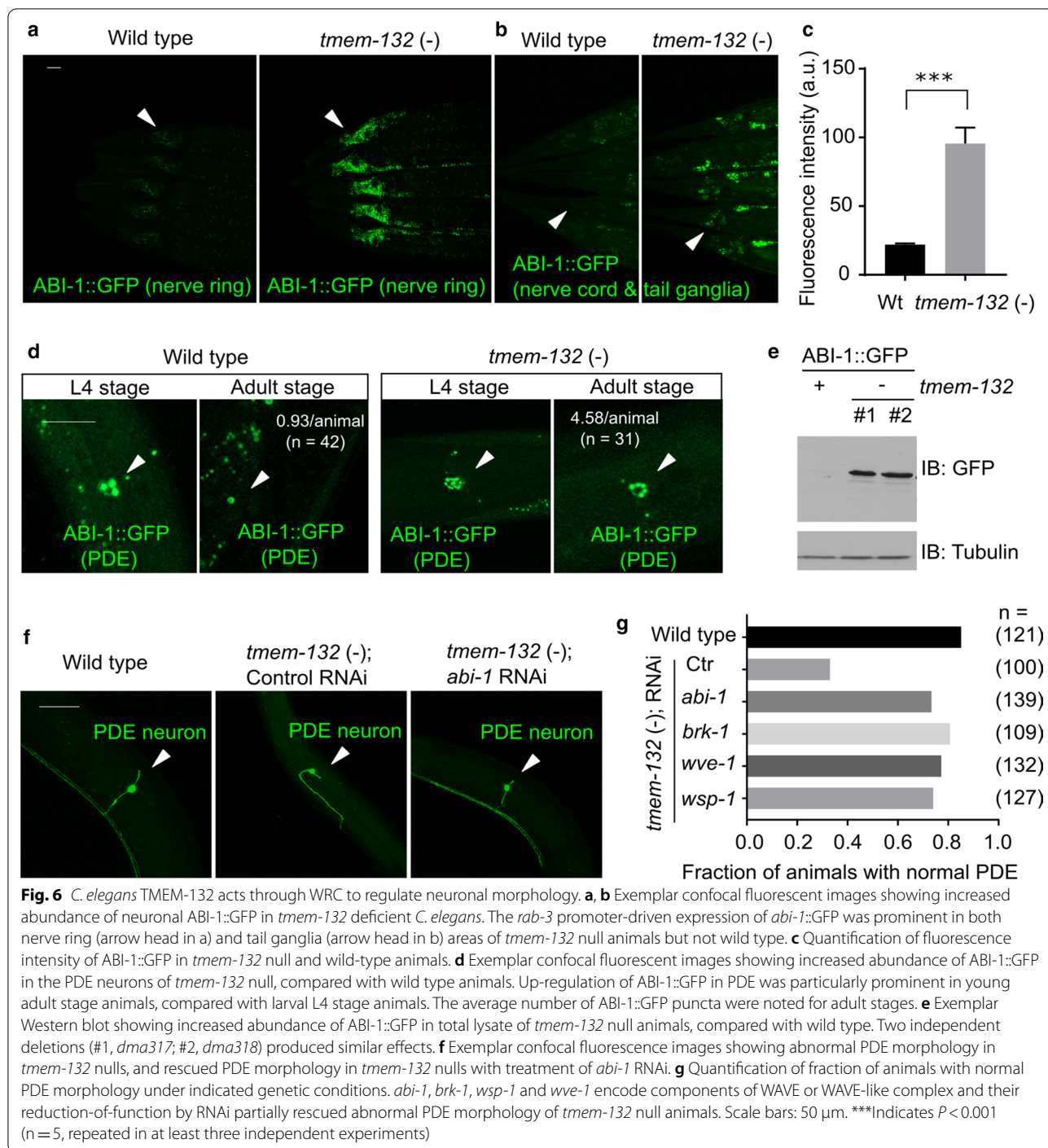
in TMEM132D markedly attenuated its interaction with Nap1 (Fig. 5a). Deletion of the C-terminal 60 a.a. of TMEM132D did not appear to affect the interaction, indicating that additional sites may contribute to the interaction with Nap1. We made similar observations for Sra1 (Fig. 5b), consistent with previous structural findings that Nap1 and Sra1 form an integral heterodimeric sub-complex of WRC [30]. Systematic deletion mutation analysis using Co-IP and Y2H assays underscored the importance of C termini of both *C. elegans* and human TMEM132 family proteins in interacting with Nap homologs (Fig. 5c). Since canonical WIRS binds to a composite surface formed by Sra and Abi but not Nap [16], our results suggest that TMEM132 differs from certain canonical WRC ligands, such as PCDH10, in specific interaction with WRC components, consistent with the idea that TMEM132 acts to sequester selective components of WRC rather than to recruit or activate WRC.



WRC acts downstream of TMEM-132 to regulate morphology of the PDE neurons

Since *C. elegans* TMEM-132 binds to GEX-3 as human TMEM132D binds to NAP1, we next addressed whether TMEM-132 regulates neuronal morphology via WRC in *C. elegans*. We generated an integrated transgenic

reporter with neuronal specific expression of the WRC component ABI-1 fused to GFP. We found that ABI-1::GFP in the nerve ring, along with the ganglia of the head and tail in *C. elegans*, is weakly fluorescent in wild type animals but strongly up-regulated in *tmem-132* mutants (Fig. 6a-c). Close microscopic analysis of



ABI-1::GFP specifically in PDE neurons revealed that ABI-1::GFP forms puncta, which decrease in numbers from the larval to adult stages in wild type animals (Fig. 6d). By contrast, numbers of ABI-1::GFP puncta in *tmem-132* mutants remain high in both larval and adult stages. We confirmed the increased abundance of ABI-1::GFP in *tmem-132* mutants by both whole-animal

Western blot and quantitative phenotypic penetrance analysis (Fig. 6a–e). To assess whether abnormally high ABI-1::GFP abundance in *tmem-132* mutants is responsible for morphologic defects of PDE neurons, we fed *tmem-132* mutants with *E. Coli* expressing double-stranded RNAi against *abi-1* and found that morphologic defects of PDE neurons were largely normalized

(Fig. 6f and Additional file 1: Fig. S3). RNAi by feeding produces weaker loss-of-function effects in neurons than by genetic deletion of WRC component-encoding genes, which by itself can cause strong PDE morphologic defects [25]. RNAi against genes encoding other components of WRC, including *brk-1* and *wve-1*, also normalized defects of PDE neurons (Fig. 6g), supporting that abnormally high WRC activity in *tmem-132* mutants caused PDE defects. Together, these results indicate that TMEM-132 may orchestrate formation of normal PDE morphology by regulating the neuronal abundance of ABI-1 and restricting WRC activity in the PDE neuron. Interestingly, the CRISPR-mediated P784T substitution in the endogenous TMEM-132 locus caused abnormal neuronal morphology of the PDE neurons in *C. elegans* (Fig. 2f), supporting the notion that functional roles of TMEM-132 in regulating F-actin and cell morphological changes are mediated by its C-terminal interaction with GEX-3 and thereby interference of WRC and actin nucleation.

Ectopic TMEM132D expression decreases the abundance of WRC components in mammalian cells

We next examined functional consequences of ectopic *TMEM132D* expression in mammalian cells. While WRC is present in most cell-types in metazoan, expression of endogenous *TMEM132D* appears to be limited to the nervous system, based on RNA profiling of various mammalian tissues (Additional file 1: Fig. S4). Similarly, we found that expression of *C. elegans tmem-132* localizes exclusively in neurons (Fig. 1b–d). We thus established a heterologous HEK293 cell line that stably expresses exogenous V5 epitope-tagged TMEM132D to assess how ectopic expression of TMEM132D affects abundance of WRC components, actin cytoskeleton dynamics and cell motility. Quantified fluorescence signal and Western blot analyses revealed that TMEM132D-expressing cell lines markedly decreased the abundance of ABI1::GFP and WAVE2::GFP while not apparently affecting that of NAP1::GFP or SRA1::GFP, after being transfected as GFP fusion constructs in control and TMEM132D cell lines (Fig. 7a, b). NAP1 and SRA1 are essential for WRC stability and prevent other WRC components from degradation in the cell [18, 32, 33]. Specific down-regulation of ABI1::GFP and WAVE2::GFP but not NAP1 or SRA1::GFP suggests that TMEM132D likely acts to sequester NAP1 and SRA1 in a sub-complex from WRC, leading to disintegration and thus decreased activity of WRC.

To test the hypothesis that TMEM132D inhibits WRC, we used the LifeAct reporter and a wound-recovery assay to examine effects of *TMEM132D* expression on actin nucleation and cell motility, respectively. LifeAct is a

17-amino-acid polypeptide that labels filamentous actin (F-actin) structures; its fusion with GFP allows visualization and quantification of actin nucleation in eukaryotic cells [34]. We found that expression of epitope-tagged *TMEM132D* in HEK293T cells markedly reduced LifeAct::GFP signals (Fig. 7c, 7d and Additional file 1: Fig. S5). This was the case even under the condition of serum starvation, which can increase LifeAct::GFP abundance compared with the serum-containing condition (Fig. 7c). Since a constitutive CMV promoter drove the expression of LifeAct::GFP, altered abundance of LifeAct::GFP may reflect endogenous F-actin levels as unbound LifeAct::GFP is unstable and degraded [34, 35]. TMEM132D did not affect overall actin abundance based on Western blot analysis using a pan-actin antibody, indicating specific inhibitory effects of *TMEM132D* expression on F-actin but not actin monomers. In addition to overall abundance, quantitative cell population-level analysis revealed that TMEM132D also reduced the percentage of cells with strong LifeAct::GFP fluorescence while not affecting the percentage of cells with control GFP fluorescence (Fig. 7d). Furthermore, a wound-recovery assay showed that ectopic *TMEM132D*-expressing cells exhibited strongly reduced motility during the 24 and 48 h recovery phases after scratching-induced wounding in cultured cells (Fig. 7e, f). Together, these results indicate that ectopic *TMEM132D* expression may decrease actin nucleation and cell motility, supporting TMEM132D as a NAP1-binding and WRC-inhibiting protein.

Discussion

Bioinformatic analysis predicted a non-canonical cellular adhesion function for TMEM132 family proteins, connecting extracellular matrix with intracellular actin cytoskeleton [5]. We provide experimental evidence to support this prediction and demonstrate that two members of the TMEM132 protein family from humans and *C. elegans* regulate cell motility and neuronal morphology, respectively, via inhibition of WRC and actin nucleation. Together, our data support a model in which TMEM132 family proteins via their C-termini bind to and sequester Nap/Sra away from WRC, leading to disintegration and decreased abundance/activity of WRC components such as Abi/Wave, and eventually reduced level of actin nucleation in localized areas of the cell (Fig. 8). Consequently, the high abundance of TMEM132 at local cell surface compartments in wild-type cells likely endows cells, including neurons, with restricted cell motility or morphogenesis, while deficiency of TMEM132 proteins may lead to development of abnormal cell motility or ectopic morphogenesis. The extracellular part of TMEM132 family proteins contain three tandem immunoglobulin

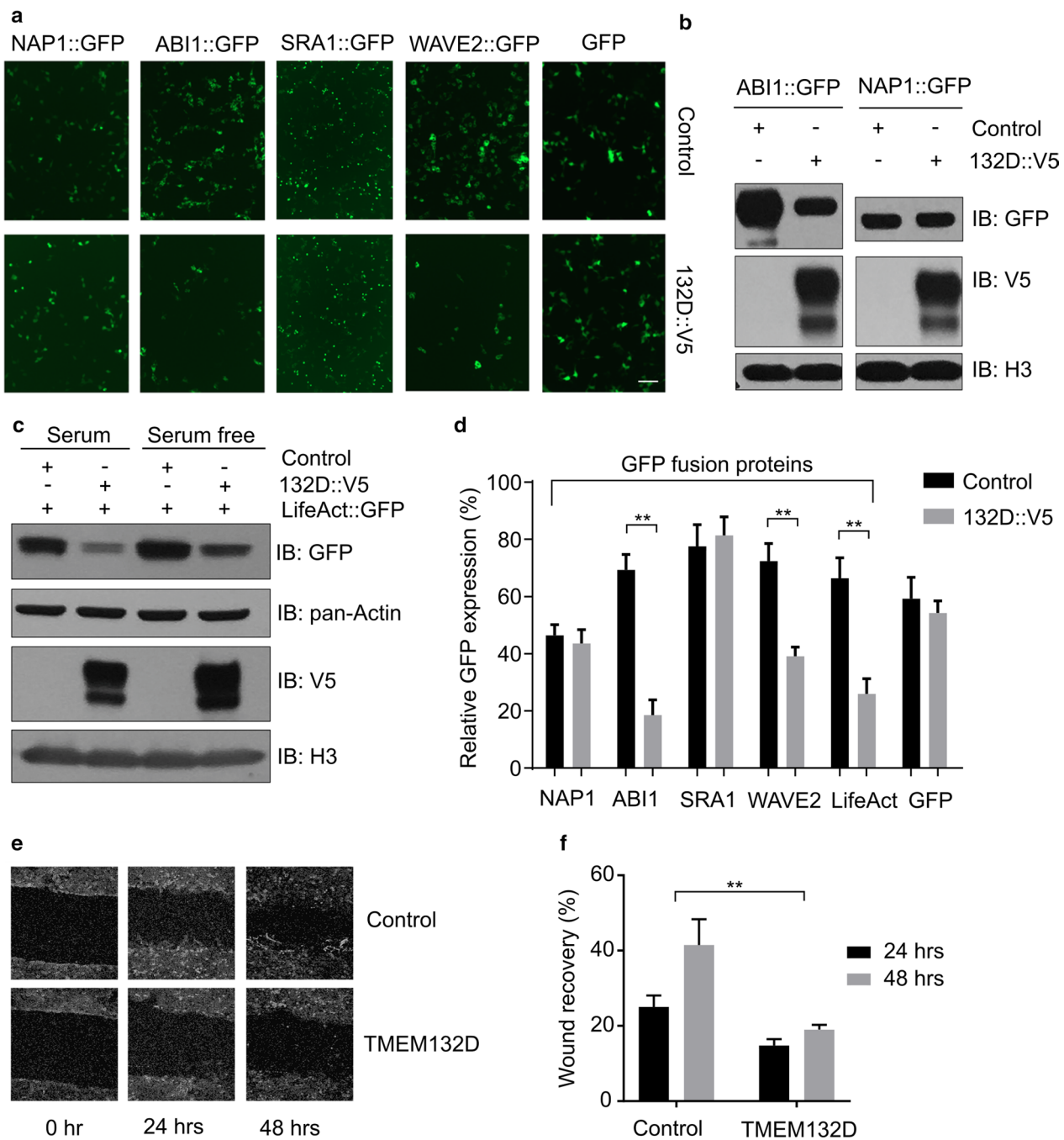
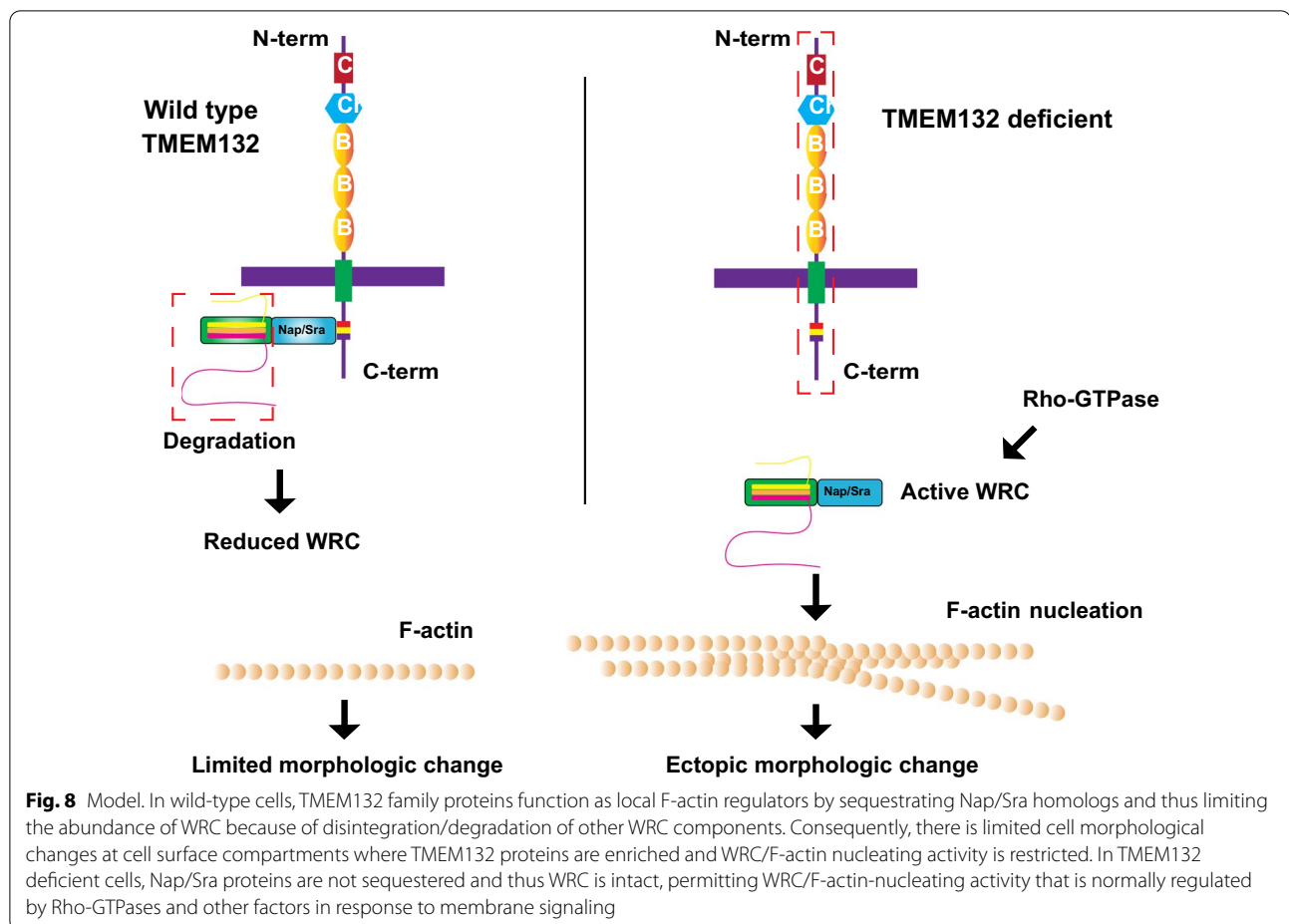


Fig. 7 TMEM132D decreases abundance of selective WAVE components. **a** Exemplar epifluorescence images showing effects of TMEM132D overexpression on abundance of GFP-tagged WAVE components in HEK293 cells. Expression constructs encoding TMEM132D and individual components of WRCs or GFP only control were co-transfected for expression and imaging at 48 h post transfection, followed by quantification of percentage of GFP + cells as shown in Fig. 7d. **b** Exemplar Western blot showing decreased abundance of ABI1 but not NAP1 by co-expression with V5-tagged TMEM132D. Comparable abundance of V5 and H3 controls effects of TMEM132D expression levels and sample loading. **c** Exemplar Western blot showing decreased abundance of LifeAct::GFP reporter by co-expression with V5-tagged TMEM132D, under serum-containing and serum-free media conditions. Comparable abundance of V5, pan-Actin and H3 controls effects of TMEM132D expression levels, monomeric Actin and sample loading respectively. **d** Quantification of percentage of GFP + cells under indicated co-transfection conditions. **e** Exemplar micrographic images showing motile recovery of HEK293 cells stably expressing control or TMEM132D after line wounding. **f** Quantification of cell-free line width indicating wound recovery in HEK293 cells stably expressing control or TMEM132D 24 and 48 h after line wounding. Scale bars: 10 μ m. **Indicates $P < 0.01$ (repeated in at least three independent experiments)



domains and a cohesin domain homolog with roles implicated in cellular adhesion [5]. How TMEM132 proteins are regulated under physiological and pathological conditions, potentially through modulation by unidentified extracellular ligands, warrants further investigation.

While major cell morphogenetic events occur during development, both human *TMEM132D* and *C. elegans tmem-132* are also highly expressed in mature neurons of the adult nervous system (Fig. 1b–d and Additional file 1: Fig. S4). Expression of the mouse homolog of *TMEM132D* is particularly high in the anterior cingulate cortex and claustral neurons, characteristic of long-range connectivity and cellular morphologic complexity [6, 36]. Similarly, PDE neurons in *C. elegans* at the lateral side of the posterior body send long-range and bifurcated axons to the anterior and posterior nerve ganglia. Neurons form synaptic connections in circuits, in which neuronal activity dynamics can induce local F-actin-dependent changes of neuronal morphology and connectivity [37–39]. Such local changes are highly regulated while most surface compartments of mature neurons remain morphologically stable, mechanically resilient

and maintained by large repertoires of cell adhesion molecules [40–42]. Correspondingly, enrichment of F-actin and actin-nucleating activity are also highly localized and differentially regulated along specific areas of cell processes and neuronal extensions, including dendritic spines, axonal synaptic termini, sensory cilia and microvilli ends [37–39, 43–45]. We propose that TMEM132 family proteins act to restrict excessive WRC and actin nucleation activities which are spatiotemporally necessary for cellular/neuronal morphological plasticity and maintenance. Emerging evidence suggests that defects in neuronal morphological development and dynamics may underlie aspects of many psychiatric disorders [46–48]. Dysfunction or dysregulation of *TMEM132D* may thus lead to abnormal neuronal structure and dynamics, contributing to heightened risks for depression, anxiety and panic disorders.

Materials and methods

C. elegans strains

C. elegans strains were maintained with standard procedures unless otherwise specified. The N2 Bristol strain

was used as the reference wild type. The genetic and transgenic alleles described in this study include Chr. III: *tmem-132(dma313)*, *tmem-132(dma317)*, *tmem-132(dma318)*, *tmem-132(dma319)*, *tmem-132(dma348)*; *dmaEx471* [*tmem-132p::tmem-132 fl::GFP*]; *lqls2* [*osm-6p::GFP*]; *dmaEx452* [*osm-6p::abi-1::GFP*; *unc-54p::mCherry*]; *dmaIs65* [*rab-3p::abi-1::GFP*; *unc-54p::mCherry*]; *dmaIs86* [*osm-6p::abi-1::GFP*; *unc-54p::mCherry*]; *dmaIs91* [*osm-6p::tmem-132::GFP*]; *wyIs592* [*ser-2p3::myr-GFP*; *odr-1p::mCherry*]; *otIs181* [*dat-1p::mCherry + ttx-3p::mCherry*]; *kyIs140* [*str-2p::GFP + lin-15(+)*].

Yeast two hybrid assay and screen

The cDNA coding sequence of the C-terminal domain of human TMEM132D was cloned into the pGBKT7 vector and screened with a normalized universal human cDNA library (Clontech, 630,481) in pGADT7 Vector, following instructions in the Matchmaker[®] Gold Yeast Two-Hybrid System (Clontech, 630,489). Verification of positive colonies was achieved by co-transformation of extracted bait and prey plasmids following the instruction of YeastMaker[™] Yeast Transformation System 2 (Clontech, 630,439) and by bait/prey plasmids with re-cloned cDNA.

Co-immunoprecipitation and Western blot

HEK293T cells transfected with mammalian expression plasmids were pelleted by centrifugation, washed once with ice-cold PBS and lysed on ice for 30 min in lysis buffer (50 mM Tris HCl pH 8, 150 mM NaCl, 0.75% NP-40, 0.5% sodium deoxycholate) or Cell Lysis Buffer (Cell Signaling Technology, 9803S) supplemented with protease inhibitor cocktail (Sigma, 11,836,153,001) and phosphatase inhibitor cocktail (Bimake, B15001). Following centrifugation at 12,000 rpm at 4 °C for 15 min, supernatants were recovered. 10% volume of whole cell lysates were collected as input. Lysates were incubated with control (Chromotek) or rabbit IgG beads (Fisher Scientific, 88,802) for pre-clear at 4 °C for 45 min. Supernatants were recovered and incubated with mCherry-Trap, GFP-Trap (Chromotek) or V5 magnetic beads (MBL International, M167-11) at 4 °C for 2 h. The beads were washed five times by lysis buffer and boiled with SDS sample buffer (Bio-rad, 1,610,747), then separated on 4–15% SDS-PAGE gel (Bio-Rad, 4,561,086) together with input. The proteins were transferred to a nitrocellulose membrane (Bio-Rad, 1,620,167) and detected using the GFP (Santa Cruz Biotechnology, sc-9996) or V5 (EMD Millipore, AB3792) antibody.

Confocal and epifluorescence microscopic imaging

SPE confocal (Leica) and digital automated epifluorescence microscopes (EVOS, Life Technologies) were used to capture fluorescence images. Animals were randomly picked at the same stage and treated with 1 mM Levamisole sodium Azide in M9 solution (31,742-250MG, Sigma-Aldrich), aligned on a 4% agar pad on a slide for imaging. Identical setting and conditions were used to compare experimental groups with control. For quantification of GFP fluorescence animals were outlined and quantified by measuring gray values using the ImageJ software. The data were plotted and analyzed by using GraphPad Prism7.

Mammalian cell culture and wound recovery assay

U2OS and HEK293T cells were cultured in DMEM (Thermo Fisher Scientific, MT-10–013-CV), supplemented with 10% fetal bovine serum (FBS, Gemini Bio-Products, 900–208) and 1% penicillin/streptomycin in a humidified 5% CO₂ incubator at 37 °C. Stably expressing TMEM132D::V5 or the control U2OS cells were constructed for wound recovery assay according to the reported protocol [49]. Cells were plated onto the 6-well plate and grew for 16 h to create a confluent monolayer, then cells were washed once by DMEM and cultured in scratch medium (DMEM supplemented with 0.5% FBS and 1% penicillin/streptomycin) for 24 h. The cell monolayer was scraped in a straight line to create a “scratch” with a P200 pipet tip. The debris was removed by washing the cells three times with DMEM medium (0 h). The cells were then cultured for 24 h in scratch medium and imaged at 0 h, 24 h and 48 h. Human excitatory neurons were derived from inducible neurogenin-2 (Ngn2) iPSC (i3N iPSCs) as described previously [50]. Briefly, i3N iPSCs were pre-differentiated in KnockOut DMEM/F12 complemented with 2 mg/ml doxycycline, 1 mg/ml mouse Laminin, 10 ng/ml BDNF, 10 ng/ml NT3, 1 × N-2 and 1 × NEAA for 3 days. Media was changed daily with 10 mM Rock inhibitor added only for the first day. After that, the pre-differentiated precursor cells were dissociated with accutase and re-plated into poly-L-lysine coated plates in maturation media which is composed of DMEM/F12: Neurobasal-A/1:1, 2 mg/ml doxycycline, 1 mg/ml mouse Laminin, 10 ng/ml BDNF, 10 ng/ml NT3, 0.5 × N-2, 0.5 × B-27, 0.5 × GlutaMax and 1 × NEAA. Half of the media was replaced every week thereafter without doxycycline supplemented. Human excitatory neurons were infected with lenti-virus (MOI = 1) for 24 h on day 2 of pre-differentiation step. The precursor cells were then re-plated onto coverslips for differentiation into mature neurons and sample replicates were fixed every 3 days for immunohistochemistry.

Statistical analysis

Data are presented as means \pm S.D. with p values calculated by one-way or two-way ANOVA. Data with non-normal distribution, including gene expression and phenotypic penetrance results, were assessed by nonparametric Mann–Whitney and Fisher's exact test, respectively.

Supplementary Information

The online version contains supplementary material available at <https://doi.org/10.1186/s13041-021-00767-w>.

Additional file 1: Fig. S1. *C. elegans* TMEM-132 is a member of the evolutionarily conserved TMEM132 protein family. **Fig. S2.** *C. elegans* TMEM-132 maintains morphologically complex PVD, ADE but not AWC neurons. **Fig. S3** Efficacy of RNAi in neurons by feeding from bacteria. **Fig. S4.** Enrichment of mammalian *TMEM132D* expression in the brain and claustral neurons. **Fig. S5.** TMEM132D regulates F-actin abundance.

Additional file 2: Table S1. List of genes encoding putative TMEM132D interactors identified from yeast-two-hybrid screens.

Acknowledgements

We thank the *Caenorhabditis* Genetics Center and the Bargmann, Hobert, Sengupta and Shen laboratories for various *C. elegans* strains, Dr. Orion Weiner's laboratory at UCSF for WRC fluorescent reporter constructs, and Dr. Li Gan's laboratory at the Gladstone Institute and UCSF for iPSC lines.

Authors' contributions

DM, YS, YD served as scientific advisors. XW, WJ, SL, BW, XY, CW collected, analyzed and presented data. XW, DM, SL, BW participated in writing and editing of the manuscript. All authors read and approved the final manuscript.

Funding

The work was supported by NIH grants R01GM117461, Pew Scholar Award, Packard Fellowship in Science and Engineering (D.K.M), a fellowship from China Scholarship Council (X.W) and a China Postdoctoral Foundation fellowship (W.J.). No funding body is involved in the design of the study and collection, analysis, and interpretation of data and in writing the manuscript.

Availability of data and materials

Data sharing not applicable to this article as no datasets were generated or analyzed during the current study.

Declarations

Ethics approval and consent to participate

Not applicable.

Consent for publication

Not applicable.

Competing interests

The authors declare that they have no competing interests.

Author details

¹ Cardiovascular Research Institute and Department of Physiology, University of California San Francisco, San Francisco, CA 94158, USA. ² State Key Laboratory for Conservation and Utilization of Bio-Resources in Yunnan, Yunnan University, Kunming 650091, Yunnan, China. ³ Key Laboratory of Metabolism and Molecular Medicine, the Ministry of Education, Department of Biochemistry and Molecular Biology, School of Basic Medical Sciences, Shanghai Medical College of Fudan University, Fudan University, Shanghai 200032, China. ⁴ Institute for Human Genetics, Department of Neurology, University of California San Francisco, San Francisco, CA 94158, USA.

Received: 26 December 2020 Accepted: 3 March 2021

Published online: 16 March 2021

References

- Kim W, Underwood RS, Greenwald I, Shaye DD. OrthoList 2: a new comparative genomic analysis of human and *Caenorhabditis elegans* genes. *Genetics*. 2018;210:445–61.
- Pandey AK, Lu L, Wang X, Homayouni R, Williams RW. Functionally enigmatic genes: a case study of the brain ignorome. *PLoS ONE*. 2014;9:e88889.
- C. elegans Sequencing Consortium. Genome sequence of the nematode *C. elegans*: a platform for investigating biology. *Science*. 1998;282:2012–8.
- Hillier LW, Coulson A, Murray JI, Bao Z, Sulston JE, Waterston RH. Genomics in *C. elegans*: so many genes, such a little worm. *Genome Res*. 2005;15:1651–60.
- Sanchez-Pulido L, Ponting CP. TMEM132: an ancient architecture of cohesion and immunoglobulin domains define a new family of neural adhesion molecules. *Bioinforma Oxf Engl*. 2018;34:721–4.
- Erhardt A, Czibere L, Roeske D, Lucae S, Unschuld PG, Ripke S, et al. TMEM132D, a new candidate for anxiety phenotypes: evidence from human and mouse studies. *Mol Psychiatry*. 2011;16:647–63.
- Erhardt A, Akula N, Schumacher J, Czamara D, Karbalai N, Müller-Myhsok B, et al. Replication and meta-analysis of TMEM132D gene variants in panic disorder. *Transl Psychiatry*. 2012;2:e156.
- Hodgson K, Almsy L, Knowles EEM, Kent JW, Curran JE, Dyer TD, et al. Genome-wide significant loci for addiction and anxiety. *Eur Psychiatry J Assoc Eur Psychiatr*. 2016;36:47–54.
- Howe AS, Buttenschön HN, Bani-Fatemi A, Maron E, Otowa T, Erhardt A, et al. Candidate genes in panic disorder: meta-analyses of 23 common variants in major anxiogenic pathways. *Mol Psychiatry*. 2016;21:665–79.
- Inoue A, Akiyoshi J, Muronaga M, Masuda K, Aizawa S, Hirakawa H, et al. Association of TMEM132D, COMT, and GABRA6 genotypes with cingulate, frontal cortex and hippocampal emotional processing in panic and major depressive disorder. *Int J Psychiatry Clin Pract*. 2015;19:192–200.
- Quast C, Altmann A, Weber P, Arloth J, Bader D, Heck A, et al. Rare variants in TMEM132D in a case-control sample for panic disorder. *Am J Med Genet Part B Neuropsychiatr Genet Off Publ Int Soc Psychiatr Genet*. 2012;159B:896–907.
- Shimada-Sugimoto M, Otowa T, Miyagawa T, Khor S-S, Omae Y, Toyo-Oka L, et al. Polymorphisms in the TMEM132D region are associated with panic disorder in HLA-DRB1*13:02-negative individuals of a Japanese population. *Hum Genome Var*. 2016;3:16001.
- Qanbari S, Pausch H, Jansen S, Somel M, Strom TM, Fries R, et al. Classic selective sweeps revealed by massive sequencing in cattle. *PLOS Genet*. 2014;10:e1004148.
- Cao J, Packer JS, Ramani V, Cusanovich DA, Huynh C, Daza R, et al. Comprehensive single-cell transcriptional profiling of a multicellular organism. *Science*. 2017;357:661–7.
- Fagerberg L, Hallström BM, Oksvold P, Kampf C, Djureinovic D, Odeberg J, et al. Analysis of the human tissue-specific expression by genome-wide integration of transcriptomics and antibody-based proteomics. *Mol Cell Proteomics MCP*. 2014;13:397–406.
- Chen B, Brinkmann K, Chen Z, Pak CW, Liao Y, Shi S, et al. The WAVE regulatory complex links diverse receptors to the actin cytoskeleton. *Cell*. 2014;156:195–207.
- Chia PH, Chen B, Li P, Rosen MK, Shen K. Local F-actin network links synapse formation and axon branching. *Cell*. 2014;156:208–20.
- Eden S, Rohatgi R, Podtelejnikov AV, Mann M, Kirschner MW. Mechanism of regulation of WAVE1-induced actin nucleation by Rac1 and Nck. *Nature*. 2002;418:790–3.
- Suzuki T, Nishiyama K, Yamamoto A, Inazawa J, Iwaki T, Yamada T, et al. Molecular cloning of a novel apoptosis-related gene, human Nap1 (NCKAP1), and its possible relation to Alzheimer disease. *Genomics*. 2000;63:246–54.
- Anazi S, Maddirevula S, Salpietro V, Asi YT, Alsahli S, Alhashem A, et al. Expanding the genetic heterogeneity of intellectual disability. *Hum Genet*. 2017;136:1419–29.
- Freed D, Pevsner J. The contribution of mosaic variants to autism spectrum disorder. *PLoS Genet*. 2016;12:e1006245.

22. Richardson CE, Shen K. Neurite development and repair in worms and flies. *Annu Rev Neurosci*. 2019. <https://doi.org/10.1146/annurev-neuro-070918-050208>.
23. Inberg S, Meledin A, Kravtsov V, Iosilevskii Y, Oren-Suissa M, Podbilewicz B. Lessons from worm dendritic patterning. *Annu Rev Neurosci*. 2019. <https://doi.org/10.1146/annurev-neuro-072116-031437>.
24. Tang NH, Jin Y. Shaping neurodevelopment: distinct contributions of cytoskeletal proteins. *Curr Opin Neurobiol*. 2018;51:11–8.
25. Shakir MA, Jiang K, Struckhoff EC, Demarco RS, Patel FB, Soto MC, et al. The Arp2/3 activators WAVE and WASP have distinct genetic interactions with Rac GTPases in *Caenorhabditis elegans* axon guidance. *Genetics*. 2008;179:1957–71.
26. Sulston J, Dew M, Brenner S. Dopaminergic neurons in the nematode *Caenorhabditis elegans*. *J Comp Neurol*. 1975;163:215–26.
27. Lamkin ER, Heiman MG. Coordinated morphogenesis of neurons and glia. *Curr Opin Neurobiol*. 2017;47:58–64.
28. Singhvi A, Shaham S. Glia-neuron interactions in *Caenorhabditis elegans*. *Annu Rev Neurosci*. 2019. <https://doi.org/10.1146/annurev-neuro-070918-050314>.
29. Welch MD, Mullins RD. Cellular control of actin nucleation. *Annu Rev Cell Dev Biol*. 2002;18:247–88.
30. Chen Z, Borek D, Padrick SB, Gomez TS, Metlagel Z, Ismail AM, et al. Structure and control of the actin regulatory WAVE complex. *Nature*. 2010;468:533–8.
31. Soto MC, Qadota H, Kasuya K, Inoue M, Tsuboi D, Mello CC, et al. The GEX-2 and GEX-3 proteins are required for tissue morphogenesis and cell migrations in *C. elegans*. *Genes Dev*. 2002;16:620–32.
32. Davidson AJ, Ura S, Thomason PA, Kalna G, Insall RH. Abi is required for modulation and stability but not localization or activation of the SCAR/WAVE complex. *Eukaryot Cell*. 2013;12:1509–16.
33. Kunda P, Craig G, Dominguez V, Baum B. Abi, Sra1, and Kette control the stability and localization of SCAR/WAVE to regulate the formation of actin-based protrusions. *Curr Biol CB*. 2003;13:1867–75.
34. Riedl J, Crevenna AH, Kessenbrock K, Yu JH, Neukirchen D, Bista M, et al. Lifeact: a versatile marker to visualize F-actin. *Nat Methods*. 2008;5:605–7.
35. Kumari A, Kesarwani S, Javoor MG, Vinothkumar KR, Sirajuddin M. Structural insights into actin filament recognition by commonly used cellular actin markers. *EMBO J*. 2020;39:e104006.
36. Saunders A, Macosko EZ, Wysoker A, Goldman M, Krienen FM, de Rivera H, et al. Molecular diversity and specializations among the cells of the adult mouse brain. *Cell*. 2018;174(1015–1030):e16.
37. Bertling E, Hotulainen P. New waves in dendritic spine actin cytoskeleton: From branches and bundles to rings, from actin binding proteins to post-translational modifications. *Mol Cell Neurosci*. 2017;84:77–84.
38. Luo L. Actin cytoskeleton regulation in neuronal morphogenesis and structural plasticity. *Annu Rev Cell Dev Biol*. 2002;18:601–35.
39. Dillon C, Goda Y. The actin cytoskeleton: integrating form and function at the synapse. *Annu Rev Neurosci*. 2005;28:25–55.
40. Diz-Muñoz A, Weiner OD, Fletcher DA. In pursuit of the mechanics that shape cell surfaces. *Nat Phys*. 2018;14:648–52.
41. Zipursky SL, Sanes JR. Chemoaffinity revisited: dscams, protocadherins, and neural circuit assembly. *Cell*. 2010;143:343–53.
42. Shapiro L, Love J, Colman DR. Adhesion molecules in the nervous system: structural insights into function and diversity. *Annu Rev Neurosci*. 2007;30:451–74.
43. Willig KI, Steffens H, Gregor C, Herholt A, Rossner MJ, Hell SW. Nanoscopy of filamentous actin in cortical dendrites of a living mouse. *Biophys J*. 2014;106:L01–03.
44. Balasanyan V, Watanabe K, Dempsey WP, Lewis TL, Trinh LA, Arnold DB. Structure and function of an actin-based filter in the proximal axon. *Cell Rep*. 2017;21:2696–705.
45. Drummond ML, Li M, Tarapore E, Nguyen TTL, Barouni BJ, Cruz S, et al. Actin polymerization controls cilia-mediated signaling. *J Cell Biol*. 2018;217:3255–66.
46. Forrest MP, Parnell E, Penzes P. Dendritic structural plasticity and neuropsychiatric disease. *Nat Rev Neurosci*. 2018;19:215–34.
47. Bernardinelli Y, Nikonenko I, Muller D. Structural plasticity: mechanisms and contribution to developmental psychiatric disorders. *Front Neuroanat*. 2014. <https://doi.org/10.3389/fnana.2014.00123/>.
48. Cristino AS, Williams SM, Hawi Z, An J-Y, Bellgrove MA, Schwartz CE, et al. Neurodevelopmental and neuropsychiatric disorders represent an interconnected molecular system. *Mol Psychiatry*. 2014;19:294–301.
49. Liang C-C, Park AY, Guan J-L. In vitro scratch assay: a convenient and inexpensive method for analysis of cell migration in vitro. *Nat Protoc*. 2007;2:329–33.
50. Wang C, Ward ME, Chen R, Liu K, Tracy TE, Chen X, et al. Scalable production of iPSC-derived human neurons to identify tau-lowering compounds by high-content screening. *Stem Cell Rep*. 2017;9:1221–33.

Publisher's Note

Springer Nature remains neutral with regard to jurisdictional claims in published maps and institutional affiliations.

Ready to submit your research? Choose BMC and benefit from:

- fast, convenient online submission
- thorough peer review by experienced researchers in your field
- rapid publication on acceptance
- support for research data, including large and complex data types
- gold Open Access which fosters wider collaboration and increased citations
- maximum visibility for your research: over 100M website views per year

At BMC, research is always in progress.

Learn more biomedcentral.com/submissions

